

Spectroscopic Measurement of High-Density CO₂-Laser-Driven Implosion

Allan Hauer, K. B. Mitchell, D. B. van Hulsteyn, T. H. Tan,
E. J. Linnebur, and M. M. Mueller

Los Alamos Scientific Laboratory, University of California, Los Alamos, New Mexico 87545

and

Paul C. Kepple

Naval Research Laboratory, Washington, D. C. 20375

and

Hans R. Griem

University of Maryland, College Park, Maryland 20742

(Received 4 August 1980)

CO₂-laser-driven implosions have been shown to produce compressed plasma densities of the same magnitude as ordinary solids ($> 2 \text{ g/cm}^3$). A variety of diagnostic techniques has been used, including the simultaneous observation of x-ray spectroscopic signatures and nuclear yield. The laser energy on target ranged from 3 to 6 kJ and the half width of the pulse was 600–800 ps. The results of these experiments are compared with numerical hydrodynamic simulations.

PACS numbers: 52.70.-m, 32.30.Rj, 52.55.Mg

The basic target employed in these experiments consisted of a thin-wall ($\sim 1\text{-}\mu\text{m}$) glass shell, 200–300 μm in diameter, coated with 10–100 μm of plastic and filled typically with 30 atm of DT seeded with 0.2–0.4 atm of argon. The thick layer of plastic reduces the fast electron preheat of the fuel. In earlier work of this type (with seeded fuel),^{1,2} only the thin glass shell was present. Long-mean-free-path electrons tended to uniformly heat and thus explode this shell. In the present work, the thick plastic has allowed a slower, more ablative implosion and considerably higher densities have been reached. Similar studies with a Nd:glass laser have recently appeared in the literature.³

The following general categories of diagnostics were employed: (a) x-ray spectroscopy, (b) x-ray imaging, (c) particle (ion) detection, and (d) nuclear product measurements. X-ray spectra were the primary diagnostic of density with x-ray imaging providing corroboration.

In Fig. 1, we show the general appearance of argon emission from progressively higher densities. Generally, the width of the argon lines is an indicator of compressed density (larger width implying higher density). The top trace was taken with an exploding pusher target and represented a compressed electron density of about $9 \times 10^{22} \text{ cm}^{-3}$. The middle trace was obtained from a target with a coating of 25- μm CH₂ (and 4.5-kJ laser energy on target). The compressed electron density here is about $4 \times 10^{23} \text{ cm}^{-3}$. The final trace

was produced by a target with 50- μm CH₂ coating and about 5.8 kJ of laser energy. The compressed electron density is about $7 \times 10^{23} \text{ cm}^{-3}$.

In the experiment represented by the top trace

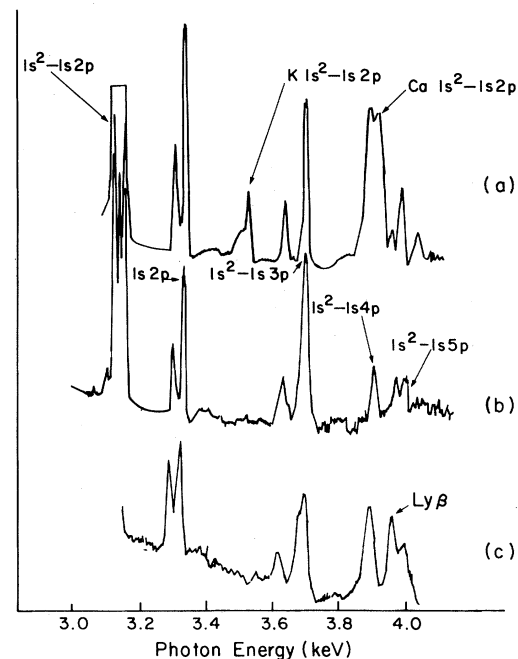


FIG. 1. Argon emission from progressively higher-density CO₂-laser-driven implosions. (a) Glass microballoon without plastic coating, (b) microballoon coated with 25 μm CH₂, and (c) microballoon coated with 50 μm CH₂. Unmarked lines are from argon.

of Fig. 1, the laser heats the glass shell directly. Lines due to calcium and potassium, which are impurities in the glass, are excited. When a layer of about 25 μm of plastic is added these lines are suppressed.

For the argon fill pressures used, Lyman β and $1s^2-1s3p$ can be considered optically thin with line center optical depths τ_0 of about 0.25-0.50. Lyman α and $1s^2-1s2p$ are quite thick with τ_0 estimated to be between 80-150.⁴

As can be seen in Fig. 1, heliumlike emission tended to be dominant in these spectra. The $1s^2-1s3p$ line, being optically thin and uncompromised by nearby lines, has been an important source of information on electron density. The densities reached by these targets are such that the line still displays a strong asymmetry (due primarily to the forbidden component on the low-energy wing). At higher densities ($>1 \times 10^{24} \text{ cm}^{-3}$) the line will blend into a Lyman- β hydrogenlike profile.

Two $1s^2-1s3p$ profile fits for electron densities of 5 and $7 \times 10^{23} \text{ cm}^{-3}$ are shown in Fig. 2. The theoretical curves (for these Stark broadened profiles) have been convolved with the spectrograph instrument profile (which contributed a broadening of about 3 eV). As is usual, the dip near line center is shallower in the experimental curves (which may be partially explained by the lack of dynamical corrections⁵ to the theoretical profile).

Density has also been measured by using other lines in the spectrum. In the early stages of this work, the temperature was too low to obtain good Lyman- γ hydrogenlike profiles. Later work at somewhat higher laser energies produced useable Lyman- γ emission. In Fig. 3 we show comparisons of density measurements made using both $1s^2-1s4p$ and Lyman γ . Unfortunately, through-

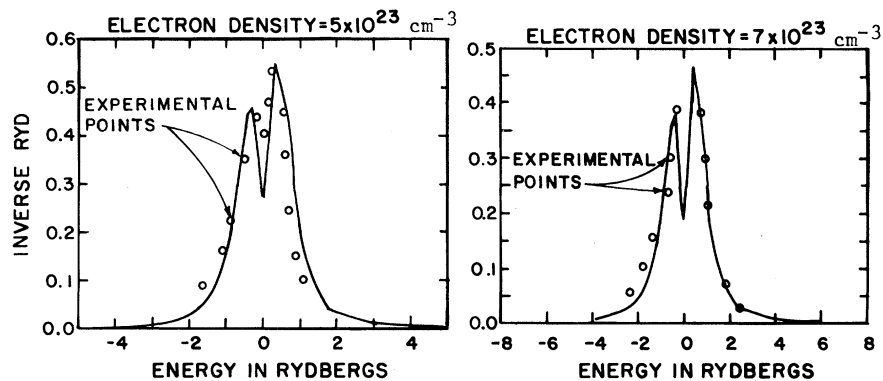


FIG. 2. Fitting of experimental to theoretical profiles for the argon $1s^2-1s3p$ line at two different densities.

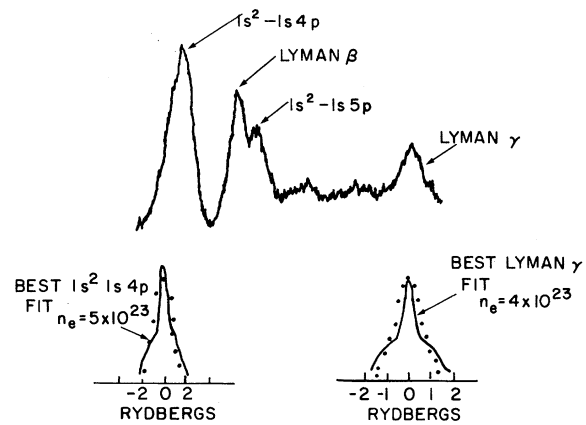


FIG. 3. Fitting of experimental to theoretical profiles for the argon $1s^2-1s4p$ and Lyman- γ lines.

out the temperature range in these experiments, $1s^2-1s5p$ severely distorted Lyman β and therefore permitted only qualitative interpretation.

All of the density and temperature measurement techniques suffer from the fact that they are integrations over time and space. Although the line emission tends to occur in a relatively small time interval near peak compression, there certainly is a finite variation in density during emission. We must thus recognize that the density evaluations are, in some sense, a measurement of "average" compressed density.

For the calculation of hydrogenlike argon profiles at densities under 10^{24} cm^{-3} , the uncertainties in the overall profile should be no more than about 20%.⁵ The error in calculating He-like profiles is somewhat greater.⁶ Uncertainties can be due to the values used for atomic energy levels, coupling of singlet and triplet states, and dynamical corrections. The errors, however, should still be less than 30%.

One of the greatest advantages of line profile measurements of density is the relative insensitivity to temperature.⁵ Electron temperatures in these experiments were measured, by continuum slope and line ratios, to be in the range 600–750 eV (± 75 eV). With this accuracy of temperature measurement the variation in line profiles should result in less than 10% error in density determination.

Density values are assigned by a least-squares fit of the experimental to the theoretical profile. A careful study⁴ of (a) the fitting procedure in the presence of data noise, (b) theoretical uncertainties, and (c) the sensitivity of the overall profile fits to density changes shows that determination of density should be accurate to better than 50%.

Compressed density was also determined by spatially resolved spectroscopy. By measuring the size of the compressed core and knowing the initial fill pressure the average compressed density is determined. The spatially resolving spectrograph utilizes a slit that provides spatial resolution orthogonal to the dispersion direction. The slit opening was 20 μm (with compressed core diameters of the order of 40 μm).

By spatially resolving several lines and the continuum (in various energy regions), an indication of the temperature variation within the compressed core can be obtained.

We have unfolded the spatially resolved spectra by fitting the spatial pattern to the distribution coming from a uniformly emitting sphere. The unfolding routine takes into account the finite size of the slit.^{2,7} The model, of course, assumes spherical symmetry (the degree of symmetry is assessed with several pinhole cameras viewing from different angles). The assessment of the boundary of the emitting fuel region (with use of the unfolding procedure) is relatively insensitive to departures from radiation homogeneity within the sphere.⁷ In addition, for the cases discussed

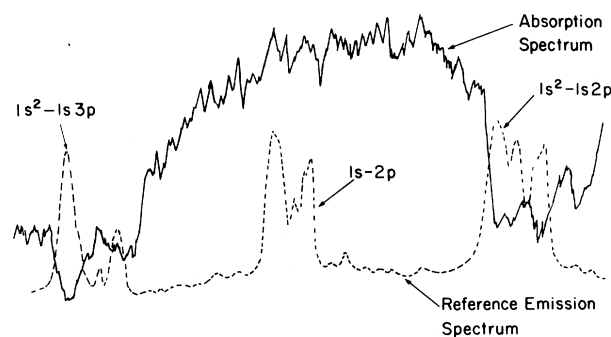


FIG. 4. Silicon absorption spectrum.

here the spatial radiation pattern matched reasonably closely that corresponding to a homogeneously emitting sphere.

An uncertainty in the compressed density measurement also occurs because of temperature gradients (causing the emission region to be different from the total compressed fuel region). This error is assessed by modeling the observed variation in source size across the spectrum (which is always small) with various temperature distributions, including those predicted by hydrodynamic simulations. Finally, an error is introduced due to the finite resolution of the slit system.

Taken in total the above uncertainties result in an accuracy of density determination of about a factor of 2. X-ray imaging can thus provide a good consistency check on spectral measurements but is not quite of the same level of accuracy.

In contrast to the thin shell explosive cases, the more ablative implosions preserve a large portion of the glass pusher in a relatively cool state (~ 250 eV). Radiation from the hot core passes out through these regions and produces absorption features in the silicon spectrum. Such a spectrum is shown in Fig. 4. A simple fitting

TABLE I. Comparison of measured and calculated parameters of laser-driven implosions. The column subheadings are SPEC, spectroscopically measured quantities; X.I., x-ray imaging; MEAS, measured; and S, simulation (theoretical calculations).

Shot No.	Target dimensions (μm)			Laser energy (J)	Electron density ($\times 10^{23} \text{ cm}^{-3}$)			Electron temperature (eV)		Neutron yield ($\times 10^7$)	
	Diam	Wall	CH ₂		SPEC	X.I.	S	SPEC	S	MEAS	S
1	230	1.3	35	4900	4.5	2	5.0	600	700	6	8
2	250	1.5	50	6284	7.5	4	7.0	750	800	10	20
3	150	1.0	37	4517	5.0	6.0	4.5	750	800	10	15

of the absorption profile of $1s^2-1s3p$ indicates a density of about $(6-7) \times 10^{23} \text{ cm}^{-3}$. Hydrodynamic simulations predict a figure closer to $9 \times 10^{23} \text{ cm}^{-3}$. More detailed analysis of such spectra offers the possibility of future direct comparisons between spectra and radio chemistry⁸ diagnostics.

The laser-driven implosions were simulated in one dimension with the Lagrangian hydrodynamics code LASNEX.⁹ The laser temporal profile used in the calculations is an accurate replica of measurements made with fast pyroelectric detectors and a 5-GHz-bandwidth oscilloscope. The hot-electron temperature is constrained to be equal to the value obtained from fast-ion measurements.¹⁰ A particularly fine zoning (of the Lagrangian grid) is used in the outer laser absorption region. In Table I, we show comparisons of experiment and theory for several important implosion parameters.

In conclusion, CO_2 -laser-driven implosions have been shown to yield high densities under conditions which also produced significant thermonuclear yield. The highest total mass densities reached in these experiments was $2-3 \text{ g/cm}^3$. With respect to inertial confinement fusion, these experiments have shown that the highly efficient CO_2 -laser driver (~ 2 overall laser efficiency) is capable of producing high-density implosions.

We would like to acknowledge many helpful discussions with Professor C. F. Hooper. We would like to thank the Los Alamos Scientific Labora-

tory target fabrication group for production of the targets used in this study. This work was performed under the auspices of the U. S. Department of Energy.

¹B. Yaakobi, D. Steel, E. Thorsos, A. Hauer, and B. Perry, *Phys. Rev. Lett.* **39**, 1526 (1977).

²K. Mitchell, D. van Hulsteyn, G. McCall, P. Lee, and H. Griem, *Phys. Rev. Lett.* **42**, 232 (1979).

³B. Yaakobi, S. Skupskys, R. L. McCrory, C. F. Hooper, H. Deckman, P. Bourke, and J. Soures, *Phys. Rev. Lett.* **44**, 1072 (1980); P. Auerbach *et al.*, *Phys. Rev. Lett.* **44**, 1672 (1980).

⁴A. Hauer, Los Alamos Scientific Laboratory Report No. LA-UR-80-1660, 1980 (unpublished). See also Proceedings of the Fifth International Conference on Spectral Line Shapes, West Berlin, Federal Republic of Germany, November 1979 (to be published).

⁵P. C. Kepple and H. R. Griem, Naval Research Laboratory Memorandum No. 3634 (1978) (unpublished); H. R. Griem, M. Blaha, and P. C. Kepple, *Phys. Rev. A* **19**, 2421 (1979).

⁶P. C. Kepple and J. Rogerson, Naval Research Laboratory Memorandum No. 4216 (1980) (unpublished).

⁷M. M. Mueller, *Bull. Am. Phys. Soc.* **24**, 1053 (1979), and Los Alamos Scientific Laboratory Report No. LA-UR-78-2698, 1978 (unpublished) (available from Mueller).

⁸F. Mayer and W. R. Rensel, KMS Fusion, Ann Arbor, Michigan Report No. U422, 1973 (unpublished).

⁹G. Zimmerman and W. Kruer, *Comments Plasma Phys.* **2**, 85 (1975).

¹⁰T. H. Tan and G. H. McCall, Los Alamos Scientific Laboratory Report No. LA-UR-80-900, 1980 (to be published).

V-Shaped Double Layers Formed by Ion Beam Reflection

R. L. Stenzel,^(a) M. Ooyama, and Y. Nakamura

Institute of Space and Aeronautical Science, University of Tokyo, Komaba, Meguro-ku, Tokyo 153, Japan

(Received 20 June 1980)

A potential double layer is observed when an ion beam is injected into a collisionless magnetoplasma along converging magnetic field lines and reflected at a positive electron-absorbing boundary. The double layer is V shaped, highly stationary, strong ($e\phi/kT_e \lesssim 25$) with amplitude determined by the beam energy ($\psi \approx V_b$), and occurs with magnetized (H_2^+) and unmagnetized (Ar^+) ions. Distribution function measurements show self-consistently formed trapped electrons on the high-potential side.

PACS numbers: 52.35.Mw, 52.40.Kh, 94.30.Kq

Potential double layers are of general interest in nonlinear plasma physics and of particular interest in space plasmas where they are thought to be the source for energetic auroral particles.¹ Double layers have been produced in the labora-

tory by various methods such as ionization processes in current-carrying discharge tubes^{2,3} or injection of drifting electron distributions from cathodes⁴ and plasma sources.⁵⁻⁷ Because of relevance to space plasmas the recent interest has